PNAS RESEARCH ARTICLE | ENVIRONMENTAL SCIENCES

Single-atom Mo–Co catalyst with low biotoxicity for sustainable degradation of high-ionization-potential organic pollutants

Zhuan Chen[a,1], Faliang An[b,1], Yayun Zhang[c], Zhiyan Liang[a], Wenyuan Liu[a], and Mingyang Xing[a,c,2]

Edited by Alexis Bell, University of California, Berkeley, CA; received April 14, 2023; accepted May 23, 2023

Single-atom catalysts (SACs) are a promising area in environmental catalysis. We report on a bimetallic Co–Mo SAC that shows excellent performance in activating peroxymonosulfate (PMS) for sustainable degradation of organic pollutants with high ionization potential (IP > 8.5 eV). Density Functional Theory (DFT) calculations and experimental tests demonstrate that the Mo sites in Mo–Co SACs play a critical role in conducting electrons from organic pollutants to Co sites, leading to a 19.4-fold increase in the degradation rate of phenol compared to the $CoCl_2$–PMS group. The bimetallic SACs exhibit excellent catalytic performance even under extreme conditions and show long-term activation in 10-d experiments, efficiently degrading 600 mg/L of phenol. Moreover, the catalyst has negligible toxicity toward MDA-MB-231, Hela, and MCF-7 cells, making it an environmentally friendly option for sustainable water treatment. Our findings have important implications for the design of efficient SACs for environmental remediation and other applications in biology and medicine.

environment remediation | molybdenum cocatalysis | single-atom catalyst | electron transfer

Significance

Combined with the cocatalytic effect of single-atom molybdenum, single-atom cobalt catalysts achieved long-term and efficient degradation of organic pollutants and retained their catalytic ability even at pH = 1.0 or 13.0. The transfer of electrons from organic pollutants to cobalt sites achieved by single-atom molybdenum reduced the dissolution toxicity of metal ions, significantly expanded the range of pollutants that could be degraded by single-atom cobalt catalyst–PMS systems, and solved the electron loss of catalysts in heterogeneous Fenton-like reactions.

The treatment of organic wastewater has become an increasingly critical issue in the long-term development of society (1, 2). The depletion of fossil fuels, environmental pollution, shortages of water, and other resources are prompting efforts to treat wastewater sustainably (3, 4). The reaction between Fe^{2+} and H_2O_2 proposed by Fenton in 1894 can produce strong oxidizing free radicals which have a broad application prospect in wastewater treatment (5). In recent years, a variety of catalysts for Fenton and Fenton-like reactions were presented to overcome inherent defects of traditional Fenton reactions. But the formation of iron cement, intolerance of inorganic salts in solution, narrow pH applicable range, and nonrecovery still bother researchers for now (6–10). In addition, organic molecules in wastewater are complex, and some with high ionization potential (IP) are hard to degrade through oxidation. This is because it takes a lot of energy to remove an electron from their outer layer, making it difficult to start the process of breaking them down.

Single-atom catalysts (SACs) with excellent chemical and physical properties are emerging as a new area in the catalysis community, and it has become the most active new frontier in the CO reduction, methane oxidation, hydroformylation of propylene, water-gas shift conversion, and many other fields beyond dispute (11–14). In the field of Fenton and Fenton-like environmental chemistry, SACs can indeed improve the activation rate of active oxides such as H_2O_2, peroxymonosulfate (PMS), and so on (15–20). However, the ≡Co(III) produced after the activation reaction needs to sostenuto consume PMS for its own reduction with slow reaction rate (21–23). The reduction and oxidation rate of Co sites in the PMS system is close to 30 times under certain conditions (Eqs. **1** and **2**) (23). Furthermore, this process indirectly causes the continuous loss of electrons on the Co sites, which hinders the utilization of PMS and reactive oxygen species (ROSs) in the system. Therefore, the reaction between PMS and single-atom Co catalysts is a REDOX reaction instead of the catalytic process. This reaction leads to the short-term property of single-atom cobalt catalysts and blocks the persistent degradation of organic pollutants. In addition, transition metal SACs such as single-atom iron and cobalt are susceptible to extreme alkaline and acidic conditions. Recent studies indicated that the activity of transition metal SACs decreased in strongly alkaline or acidic solutions (20, 24–27), and the resistance of transition metal SACs in the complex environment is alarming. Therefore, it is necessary to develop a technology that can support the adaptable and long-term degradation of pollutants by single-atom cobalt catalyst at present.

$$\equiv \mathrm{Co(II)} + \mathrm{HSO_5^-} \rightarrow \equiv \mathrm{Co(III)} + \mathrm{SO_4^{\cdot -}} + \mathrm{OH^-}; \mathrm{k} = 100.0\ \mathrm{M^{-1}S^{-1}}, \quad [1]$$

$$\equiv \mathrm{Co(III)} + \mathrm{HSO_5^-} \rightarrow \equiv \mathrm{Co(II)} + \mathrm{SO_5^{\cdot -}} + \mathrm{H^+}; \mathrm{k} = 0.35\ \mathrm{M^{-1}S^{-1}}. \quad [2]$$

Author affiliations: [a]Key Laboratory for Advanced Materials and Joint International Research Laboratory of Precision Chemistry and Molecular Engineering, Feringa Nobel Prize Scientist Joint Research Center, School of Chemistry and Molecular Engineering, East China University of Science and Technology, Shanghai 200237, China; [b]State Key Laboratory of Bioreactor Engineering, East China University of Science and Technology, Shanghai 200237, China; and [c]Shanghai Engineering Research Center for Multimedia Environmental Catalysis and Resource Utilization, East China University of Science and Technology, Shanghai 200237, China

Author contributions: M.X. designed research; Z.C. performed research; F.A., Y.Z., and M.X. contributed new reagents/analytic tools; Z.C., Z.L., W.L., and M.X. analyzed data; and Z.C. and M.X. wrote the paper.

The authors declare no competing interest.

This article is a PNAS Direct Submission.

[1]Z.C. and F.A. contributed equally to this work.

[2]To whom correspondence may be addressed. Email: mingyangxing@ecust.edu.cn.

This article contains supporting information online at https://www.pnas.org/lookup/suppl/doi:10.1073/pnas.2305933120/-/DCSupplemental.

Published July 10, 2023.

This study reported on the development and testing of a single-atom catalyst, $SAMCC_{0.5}$, which contained both Mo and Co sites. The results indicated that this catalyst was robust and versatile in its ability to degrade organic pollutants, with high resistance to interference from extreme pH levels and other ionic species. The results also suggested that the Mo sites acted as a bridge to facilitate electron transfer from the organic pollutants to the Co sites, a process supported by both theoretical calculations and degradation experiments using different model contaminants with varying IPs. The long-term stability and recyclability of $SAMCC_{0.5}$ were also demonstrated through a 10-d, 30-round degradation experiment, where ROSs such as singlet oxygen ($^1O_2$) and high-valent cobalt were identified. Overall, these findings contributed to the advancement of sustainable and efficient catalytic technologies for environmental remediation.

Results

Synthesis and Characterization of $SAMCC_{0.5}$. With a simple synthesis method (Fig. 1*A*), Co and Mo atoms coordinated with 1,10-phenanthroline in mixed solution, and then, the metal atoms were fixed together with the substrate after calcination. The proportion of Co and Mo elements in the catalyst was found to be crucial and was studied through *SI Appendix*, Figs. S1 and S2. Therefore, the ratio of the Co to Mo element in the raw material was the first to be studied in *SI Appendix*, Figs. S1 and S2. In the end, the best catalyst in this series was identified as $SAMCC_{0.5}$. SAC only containing Co element was called Co–N–C.

Scanning electron microscope (*SI Appendix*, Fig. S3) and high-resolution transmission electron microscopy (HRTEM) images (Fig. 1*B* and *SI Appendix*, Fig. S4) showed that this catalyst was a porous particle with a rough surface and there was no aggregation of metal particles on the evenly distributed edge flakes. According to *SI Appendix*, Fig. S5, nitrogen adsorption and desorption isotherms of $SAMCC_{0.5}$ and Co–N–C showed that their specific surface areas were 372.3731 m^2/g and 306.2080 m^2/g, respectively. Through infrared spectroscopy in *SI Appendix*, Fig. S6, the main chemical bonds of $SAMCC_{0.5}$ and Co–N–C were C–N and C=C bonds, and there were some hydroxyl groups on the catalyst surface. The existence of C–N and C=C bonds indicated that the conjugate skeleton still existed in the $SAMCC_{0.5}$ and Co–N–C. The high-angle annular dark-field (HAADF) STEM images in Fig. 1*C* revealed that the $SAMCC_{0.5}$ sample was abundant in atomic Co and Mo sites, and most of the metal atoms were in the form of single atoms or several adjacent atoms. Mo atoms appeared slightly brighter than Co atoms in the high-angle annular dark-field image due to their larger atomic number. The ratio of Mo to Co atoms was estimated to be approximately 1:4. The X-ray diffraction (XRD) pattern, as shown in *SI Appendix*, Fig. S7, confirmed the absence of detectable amounts of crystalline Co or Mo phases, indicating that $SAMCC_{0.5}$ was substantially free of metallic Co/Mo or cobalt/molybdenum oxides. The energy dispersive X-ray spectroscopy mapping images in Fig. 1*D* showed a homogeneous distribution of Mo (represented by purple), Co (represented by indigo), and N (represented by orange) elements, demonstrating a uniform distribution of Mo and Co atoms throughout the SAMCC0.5 particles. The results from the inductively coupled plasma atomic emission spectrometry (ICP-AES), as presented in *SI Appendix*, Table S1, showed that the Co and Mo content in the catalyst were approximately 0.74% and 0.19%, respectively. As a comparison, the content of the Co element in Co–N–C was 1.00%.

The chemical state and local environment of Mo and Co were further investigated by the X-ray adsorption near edge structure (XANES) and extended X-ray absorption fine structure (EXAFS) spectra. According to *SI Appendix*, Fig. S8, the Co and Mo K-edge X-ray absorption near-edge structure (XANES) and valence analysis suggested the valence state of Co in $SAMCC_{0.5}$ including Co^{2+} and Co^{3+} states while the valence state of Mo was Mo^{6+}, combining with k-space and fitted data of Co and Mo elements in *SI Appendix*, Figs. S9 and S10. As is shown in Fig. 1*E*, the k_3-weighted Fourier-transformed extended X-ray absorption fine structure spectra (FT-EXAFS) showed that the Co element in $SAMCC_{0.5}$ was mainly coordinated with nitrogen (N) atoms, with a bond length of 1.42 Å corresponding to the Co–N bond in CoPc. Meanwhile, no obvious peaks assigned to the Co–Co bond at 2.18 Å were observed, thus implying the absence of Co clusters or crystalline particles. Moreover, for the FT-EXAFS curves of the Mo element in Fig. 1*F*, the main peaks for $SAMCC_{0.5}$ were located at 1.34 Å differing from the Mo–Mo bond located at 2.38 Å and were consistent with the location of the fitting curve for Mo–N bond. To assign the above peaks, the wavelet transform (WT) EXAFS in Fig. 1*G* was carried out for the $SAMCC_{0.5}$ sample as well as the standards. Referring to the WT-EXAFS feature of CoPc in *SI Appendix*, Fig. S11, the peak at 1.42 Å on $SAMCC_{0.5}$ could be assigned to the Co–N bond. Compared to the feature peak of Mo foil (2.38 Å, 8.66 $Å^{-1}$) in WT-EXAFS, the presence of the peak of the Mo element in SAMCC (1.38 Å, 7.78 $Å^{-1}$) excluded the existence of the Mo–Mo bond. Therefore, Mo atoms and Co atoms in $SAMCC_{0.5}$ were mainly coordinated with N atom in $SAMCC_{0.5}$.

Catalytic Effect Test. The catalytic activity of $SAMCC_{0.5}$ for Fenton-like reactions was evaluated using phenol as a model pollutant. The results in Fig. 2*A* showed that the degradation rate of phenol reached 78% in 3 min with the addition of PMS. On the other hand, the degradation rate of phenol in the presence of Co–N–C, which did not contain Mo, only reached 28%. Additionally, Mo–N–C and N–C, which lacked Co or other metal elements, were unable to effectively activate PMS. According to the Zeta potential of catalysts under different pH in *SI Appendix*, Fig. S12, negative charge existed on the surface of catalysts and the addition of phenol did not change the chemical environment which mean that the adsorption of phenol hardly existed. At the same time, the degradation of phenol in the $SAMCC_{0.5}$ system decreased sharply with the absence of PMS, which also indicated that $SAMCC_{0.5}$ could not adsorb phenol.

The use of Co^{2+} as a classical catalyst for PMS activation in Fenton-like reactions is widely established. However, few heterogeneous catalysts can match the efficiency of PMS activation of Co^{2+}, let alone surpass it. To further demonstrated the effectiveness of phenol degradation by the $SAMCC_{0.5}$–PMS system, experiments were conducted using $Co(Ac)_2$ and $CoCl_2$ as comparison catalysts. The results in Fig. 2 *B* and *C* showed that phenol was not efficiently degraded when using $Co(Ac)_2$ and $CoCl_2$ equivalent to the Co element in $SAMCC_{0.5}$. The apparent kinetic constant of the $SAMCC_{0.5}$–PMS system was 19.4 times higher than that of the $CoCl_2$–PMS system. Even when the concentration of $CoCl_2$ was increased 20 times, the degradation rate of phenol was still not as efficient as the $SAMCC_{0.5}$–PMS system. The use of Co_3O_4 as a catalyst in a Fenton-like reaction also showed limited effectiveness in oxidizing phenol, as shown in *SI Appendix*, Fig. S13. These results further demonstrated the unique advantage of the single-atom catalyst in addressing environmental pollution.

The $SAMCC_{0.5}$–PMS system was a modified version of the traditional Fenton reaction and has been used to treat phenol solutions under different pH conditions and buffer systems. It was

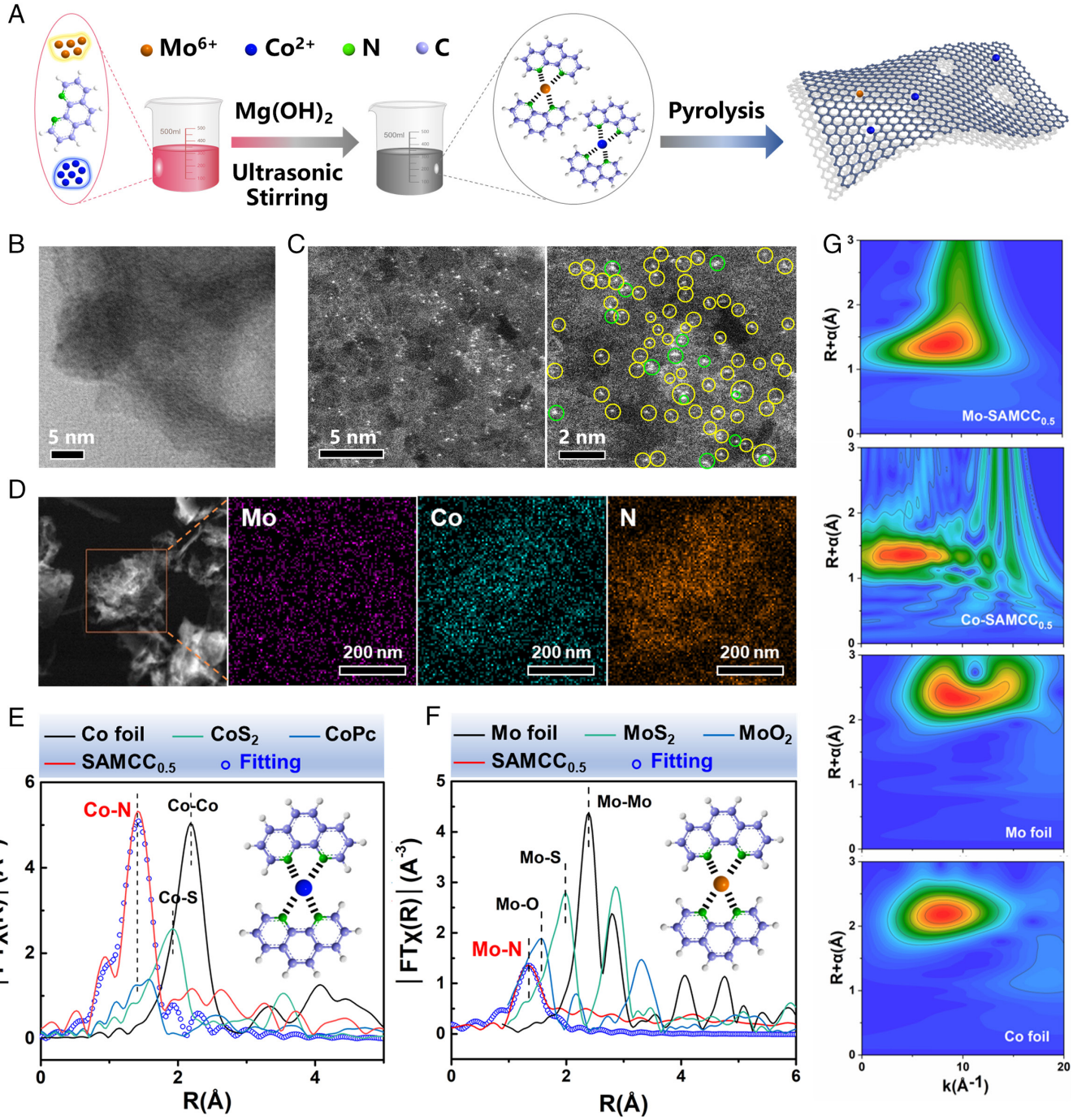

Fig. 1. (*A*) Synthesis process of $SAMCC_{0.5}$ and schematic diagram of the structure. (*B*) HRTEM image of $SAMCC_{0.5}$. (*C*) Aberration-corrected HAADF-STEM image of $SAMCC_{0.5}$: Yellow circles indicate single Co atoms, and green circles indicate single Mo atoms. The atomic number contrast indicates that the larger the atomic number, the brighter the image. Thus, atomic Mo will be brighter. (*D*) Elemental mapping for $SAMCC_{0.5}$. (*E*) EXAFS in R-space and corresponding fitting curves for Co foil, CoS_2, CoPc, and $SAMCC_{0.5}$. (*F*) EXAFS in R-space and corresponding fitting curves for Mo foil, MoS_2, MoO_2, and $SAMCC_{0.5}$. (*G*) WT-EXAFS for the Mo element of $SAMCC_{0.5}$, Co element of $SAMCC_{0.5}$, Mo foil, and Co foil.

found in Fig. 2*D* that the pH of the reaction solution had little effect on the catalytic activity of $SAMCC_{0.5}$, and the reaction rate did not decrease when phosphate buffer was used as the reaction solution (*SI Appendix*, Fig. S14). When pH was set to 12 or 13, the degradation rate of phenol decreased slightly, and the pH after reaction was 11.68 and 12.70, respectively (Fig. 2*D*). According to the pH of reaction solution after reaction, the whole process of reaction was under an alkaline environment, and the decline of the degradation rate of phenol here was probably due to the ineffective self-decomposition of PMS under alkaline environment (28, 29). To sum up, Fenton-like reaction dominated by the $SAMCC_{0.5}$–PMS system has greatly escaped the disadvantage of a narrow pH range of application.

Inspired by phosphate buffer, Na_2CO_3, $NaHCO_3$, humic acid, and other salts were used as interferences in the reaction system, and further activity tests were carried out. It can be seen from Fig. 2*E* that most of the salts and humic acid could not cause the attenuation of the activity of the $SAMCC_{0.5}$–PMS system, and the degradation rate of phenol in the $SAMCC_{0.5}$–PMS system interestingly became faster when humic acid was added as is shown

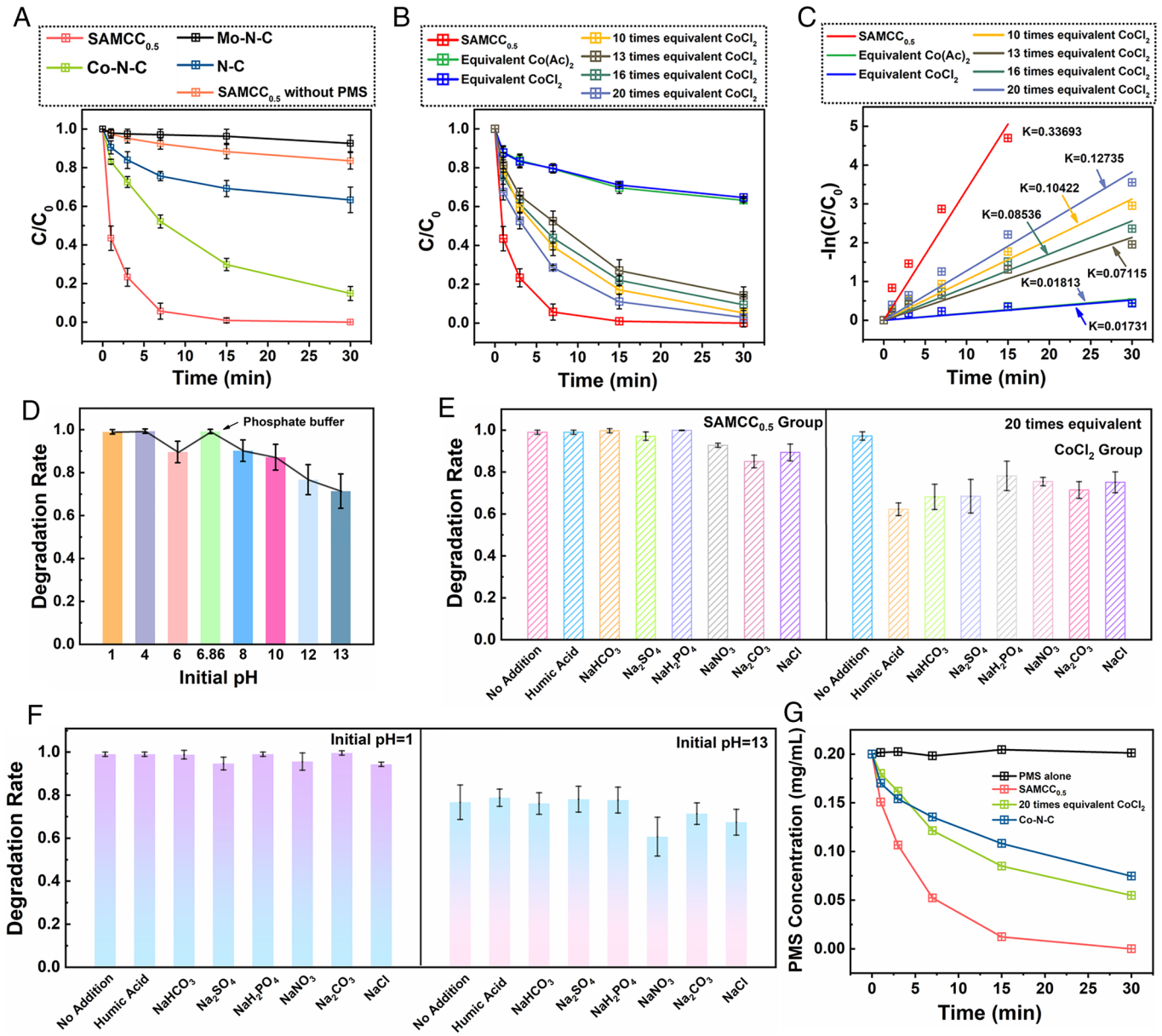

Fig. 2. (*A*) Degradation rate of phenol when $SAMCC_{0.5}$, Co–N–C, Mo–N–C and N–C were used as catalysts. (*B*) Degradation rate of phenol when 300 mg L^{-1} $SAMCC_{0.5}$ and different equivalents of $CoCl_2$ were used as catalysts. (*C*) Apparent kinetic constants of (*B*). (*D*) $SAMCC_{0.5}$ catalytic degradation rate of phenol under different pH environments. (*E*) $SAMCC_{0.5}$ and different equivalents of $CoCl_2$ catalytic degradation rate of phenol with interference of 0.2 M salts and humic acid. (*F*) $SAMCC_{0.5}$ catalytic degradation rate of phenol with interference of 0.2 M salts and humic acid with pH = 1 and 13. (*G*) Decomposition rate of PMS with the catalytic effect of $SAMCC_{0.5}$, Co–N–C and 20 times equivalent $CoCl_2$. Dosage: PMS: 200 mg L^{-1}, reaction solution: 100 mL, catalyst: 300 mg L^{-1}, reaction time: 30 min.

in *SI Appendix*, Fig. S15. In the traditional Fenton reaction, ·OH and $SO_4^{\cdot-}$, which are the main ROSs in the traditional Fenton system, easily interact with a variety of anions to generate other free radicals with weaker oxidizing potential (30, 31). In Fig. 2*E*, the degradation rate of 20 times equivalent $CoCl_2$–PMS system declined when salts and humic acid were added. Among these, humic acid, Na_2SO_4, and $NaHCO_3$ disturbed the degradation indeed. For single-atom Co catalysts, Co sites were the electron-rich region in the catalyst and cannot strongly attract various anions (18, 32). While Co^{2+} as a transition metal ion has many vacant orbitals, which is easy to coordinate with anions and results in the inactivation of Co^{2+}. In addition, it is suggested that the nonradical ROSs rather than free radicals may dominate in the $SAMCC_{0.5}$–PMS system, which could hardly be consumed by the anions. In order to further verify the stability and anti-interference ability of $SAMCC_{0.5}$ in complex actual water treatment scenarios, the degradation ability of the $SAMCC_{0.5}$–PMS system was tested under extreme pH conditions in Fig. 2*F*. Surprisingly, the degradation effect of the $SAMCC_{0.5}$–PMS system was not affected by the addition of various salts, no matter at pH = 1 or 13. After the addition of various salts, the degradation rate of phenol was all close to 100% at pH = 1. And the degradation rate of phenol at pH = 13 was not very different from that before the addition of inorganic salts, although the degradation rate of phenol could not reach 100%. Therefore, the $SAMCC_{0.5}$–PMS system maintains good resistance to interference even under extreme pH conditions. In order to further investigate the performance of the $SAMCC_{0.5}$–PMS system in complex environments, phosphate buffer solutions with different anions were used as reaction solutions. In *SI Appendix*, Fig. S16, it could be clearly seen that even in the complex environment of buffer solution, the $SAMCC_{0.5}$–PMS system was still not affected by various anionic interferences. The character that

had great anti-interference capability under wide pH environment made this system promising in the future application of actual waste treatment. Moreover, in order to further verify the ability of the catalyst to degrade pollutants in practical applications, activity tests were carried out with river water from different locations as the reaction solution. The results, shown in *SI Appendix*, Fig. S17, demonstrated that the catalyst was highly effective even when tested with river water from the Huangpu River in Shanghai, the Changjiang River in Nanjing, the Bailang River in Shandong, the Zhujiang River in Guangzhou, and running water from Shanghai. The catalyst was able to effectively degrade phenol in all these water samples, indicating its strong potential for practical use.

Therefore, the results of the degradation of phenol demonstrated that the $SAMCC_{0.5}$–PMS system outperformed traditional Fenton and Fenton-like reaction systems. The superior performance could be attributed to the higher activation rate of PMS in the $SAMCC_{0.5}$ system, as indicated by the Iodine reduction reaction. This was further supported by the results presented in Fig. 2*G* and *SI Appendix*, Fig. S18, which showed a significantly higher PMS activation rate in the $SAMCC_{0.5}$ system compared to the other two catalysts.

Possible Degradation Pathways. The degradation products of phenol in the $SAMCC_{0.5}$–PMS system were analyzed using gas chromatography–mass spectrometry (GC–MS), as illustrated in *SI Appendix*, Fig. S19. Three of the four resonance products of phenol were easy to be oxidized, and the products were catechol and hydroquinone (m/z = 110) (33, 34). Both catechol and hydroquinone were found to be more easily oxidized than phenol due to their lower ionization potential. Further oxidation of catechol and hydroquinone led to the formation of o-quinone and p-quinone (m/z = 108), followed by the oxidation of these compounds into $C_6H_6O_4$ (m/z = 142), $C_6H_4O_6$ (m/z = 172) and $C_4H_4O_4$ (m/z = 116). Ultimately, these organic compounds were oxidized to $C_2H_2O_4$ (m/z = 142), which was easily converted into CO_2 and H_2O.

Catalytic Mechanism of the $SAMCC_{0.5}$–PMS System. In the study of the Co^{2+}–PMS system, researchers have long believed that the system is dominated by the presence of ·OH and $\cdot SO_4^-$. In order to evaluate the role of ROSs in the $SAMCC_{0.5}$–PMS system, four sacrificial agents were employed in Fig. 3*A*. Tert-butanol was utilized as a limiting agent for ·OH and $\cdot SO_4^-$, while p-benzoquinone was employed to restrict the presence of $\cdot O_2^-$. However, neither of these agents showed significant inhibitory effects when used at concentrations of 2 mM or 20 mM in the $SAMCC_{0.5}$–PMS system. The use of 2,2,6,6-tetramethylpiperidine (TEMP) and dimethyl sulfoxide (DMSO) as sacrificial agents for $^1O_2$ and high-valent cobalt in the $SAMCC_{0.5}$–PMS system was found to have a significant inhibitory effect on the reaction. Both 20 mM TEMP and DMSO were shown to significantly decrease the rate of degradation of the system. The results of this experiment were consistent with the results of the electron paramagnetic resonance (EPR) test in Fig. 3*B*. When TEMP was utilized as the capture agent in the experiment, a distinct triplet peak corresponding to $^1O_2$ was observed. On the other hand, the use of 2,2-dimethyl-3,4-dihydro-2H-pyrrole 1-oxide (DMPO) as the capture agent resulted in a sevenfold peak in the EPR test, which was identified as the deep oxidation product of DMPO, (5,5-dimethyl-2-oxo-pyrroline-1-oxyl, DMPOX). It is important to note that the presence of DMPOX does not provide specific information about the types of ROSs present in the system, as various oxides can lead to the conversion of DMPO into DMPOX (35, 36). Here, ·OH was detected through the fluorescence method. According to *SI Appendix*, Fig. S20, there was a weak peak at 410 nm, which meant that the content of ·OH in the $SAMCC_{0.5}$–PMS system was small. Combining with the results of sacrificial agent experiments and EPR test, the active oxygen species dominated in the $SAMCC_{0.5}$–PMS system was still high-valent cobalt and $^1O_2$.

In order to investigate the presence of high-valent cobalt, (E)-1,2-diphenylethene was utilized as a probe molecule in degradation experiments (Fig. 3*C* and *SI Appendix*, Table S2). High-valent cobalt, which is characterized by its ability to carry out an oxygen atom transfer reaction, can oxidize (E)-1,2-diphenylethene to produce 2,3-diphenyloxirane. Although other ROSs can also react with (E)-1,2-diphenylethene, the products produced by these reactions are complex and can be differentiated from 2,3-diphenyloxirane. The probe experiment with (E)-1,2-diphenylethene showed the presence of 2,3-diphenyloxirane in both the $SAMCC_{0.5}$–PMS and Co–N–C–PMS systems. Although the proportions of 2,3-Diphenyloxirane in the products of these two systems were only 4.47% and 3.14% respectively, the low conversion rate of (E)-1,2-diphenylethene suggested the presence of a certain amount of high-valent cobalt. For the $CoCl_2$–PMS system, 2,3-Diphenyloxirane occupied a very small proportion in the product, while most of the reaction products were the outcome of (E)-1,2-Diphenylethene reacting with free radicals. Therefore, high-valent cobalt was negligible compared to other ROSs in the $CoCl_2$–PMS system.

In accordance with the above findings, it has been determined that $^1O_2$ was generated as a result of the interaction between a single-atom cobalt site and PMS. Conversely, PMS has the capability to oxidize the cobalt site, leading to the formation of high-valent cobalt in its oxidation state. This accepted series of reactions serve as a basis for understanding the generation of ROSs (Eqs. **3**–**6**) (37–39).

$$\equiv \mathrm{Co(III)} + \mathrm{HSO_5^-} \rightarrow \equiv \mathrm{Co(II)} + \mathrm{SO_5^{\cdot -}} + \mathrm{H^+}, \quad [3]$$

$$2\mathrm{SO_5^{\cdot -}} \rightarrow 2\mathrm{SO_4^{2-}} + {}^1\mathrm{O_2}, \quad [4]$$

$$\equiv \mathrm{Co(II)} + \mathrm{HSO_5^-} \rightarrow \equiv \mathrm{Co(IV)=O} + \mathrm{SO_4^{2-}} + \mathrm{H^+}, \quad [5]$$

$$\equiv \mathrm{Co(IV)=O}/{}^1 + \text{Organic pollutants} \rightarrow \equiv \mathrm{Co(III)}/\equiv \mathrm{Co(II)} + \text{Oxidation products} \quad [6]$$

From Fig. 2*A*, it was clear that the Mo–N–C catalyst alone failed to effectively activate PMS. However, the introduction of Mo enhanced the interaction between Co sites and PMS, resulting in a substantial improvement in phenol degradation. This highlighted the crucial role that Mo played as a cocatalyst in the $SAMCC_{0.5}$–PMS system. To further explore the role of Mo in the cocatalytic process, X-ray photoelectron spectroscopy (XPS) was conducted on samples of $SAMCC_{0.5}$ and Co–N–C before and after the reaction. XPS analysis of the Co element in Co–N–C as shown in Fig. 3*D* revealed a shift in the peak position of the Co element toward higher energy levels by 0.5 eV as a result of oxidation after its reaction with PMS. Notably, the XPS results of the Co element in $SAMCC_{0.5}$ in Fig. 3*E* showed a shift of 0.7 eV toward lower energy levels, indicating that the Co site in the $SAMCC_{0.5}$–PMS system has received electrons. However, the Mo, C, and N elements in $SAMCC_{0.5}$ did not change significantly before and after the reaction as is shown in *SI Appendix*, Fig. S21, and the Mo element always existed in the valence state of +6. It

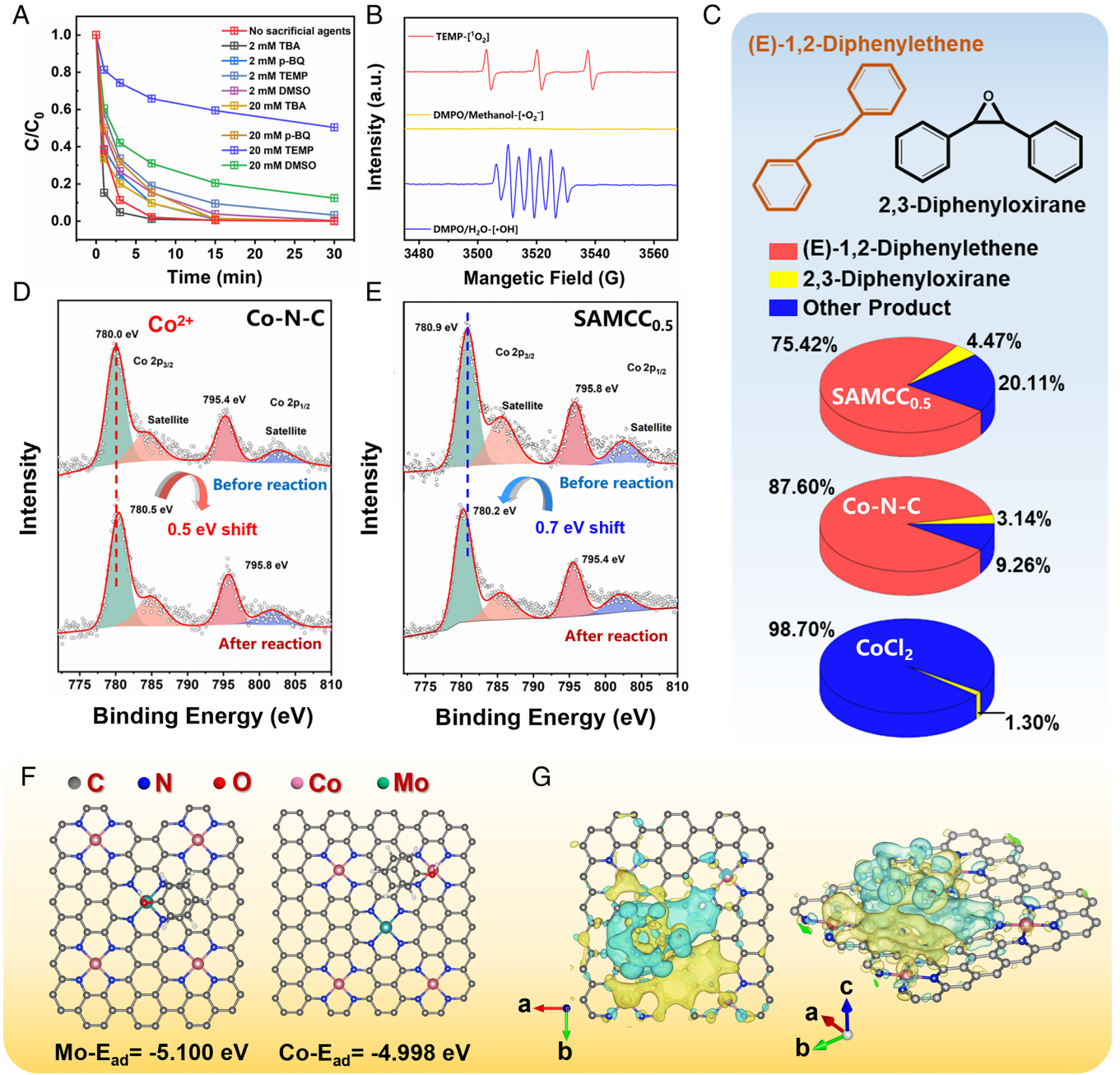

Fig. 3. (*A*) Sacrificial agent experiments. Dosage: catalyst: 300 mg L^{-1}PMS: 200 mg L^{-1}, aqueous solution: 100 mL, reaction time: 30 min. (*B*) EPR tests for the $SAMCC_{0.5}$–PMS system. (*C*) Proportion of product in (E)-1,2-Diphenylethene probe experiment with different system. (*D* and *E*) XPS results of the Co element in the Co–N–C and $SAMCC_{0.5}$ before and after reaction. (*F*) Adsorption energy of phenol on the Co and Mo sites. (*G*) Differential charge of the system after the adsorption of phenol on the Mo site.

indicated that the source of electrons transferred to the Co site was not the Mo element. Meanwhile, PMS with strong oxidizing properties can hardly reduce the Co element, and there was no obvious trace of reaction between PMS and Mo element. As such, the source of electrons was likely to be the residual organic phenol molecule present in the system.

The hypothesis was verified using DFT calculations. The adsorption energy of the model organic pollutant (phenol) on Mo/Co sites in $SAMCC_{0.5}$ was calculated in Fig. 3*F*, and the results showed that the adsorption energy of phenol to the Mo site was −5.100 eV, which was more favorable than that to the Co site (−4.998 eV). This suggested that phenol molecules are more likely to interact with Mo sites compared to Co sites. To further support the hypothesis, the differential charge of the system when phenol was adsorbed on the Mo site was calculated, as illustrated in Fig. 3*G*. The yellow regions indicated areas of increased electron density, while the cyan regions indicated areas of electron deficiency. The electron transfer path of the $SAMCC_{0.5}$–PMS system could be described as follows: phenol adsorbed on the Mo site on the catalyst surface injected its electrons into Mo, which were then transferred to the Co sites through the conjugated framework, resulting in an increase in the electron cloud density of Co after the reaction. This suggested that the electrons used for activating on the Co site primarily come from the organic pollutant of phenol and that Co itself did not lose electrons, thereby enabling cyclic degradation of phenol. These calculation results were

basically consistent with our hypothesis. The previous experiment revealed an intriguing phenomenon, where the addition of humic acid and tert-butanol did not diminish the degradation rate of phenol. Rather, humic acid and tert-butanol served as electron donors, facilitating the transfer of electrons to the Mo sites and increasing the likelihood of electrons flowing to the electron-deficient Co sites. This, in turn, allowed the Co sites to sustainably activate PMS by continuously reducing itself. According to the results obtained, it could be stated that the Mo sites played a crucial role as a bridge that facilitated electron transfer from organic pollutants to the Co sites throughout the entire conjugate structure. Additionally, the results of the electrochemical impedance spectroscopy performed on $SAMCC_{0.5}$ and Co–N–C also provided support for this conclusion. As shown in *SI Appendix*, Fig. S22, $SAMCC_{0.5}$ displayed a significantly lower electrochemical impedance compared to Co–N–C, indicating that electrons were able to flow more efficiently on $SAMCC_{0.5}$ and reinforcing the role of the Mo site as an electron conduit. $AgNO_3$ was added as a sacrificial agent to the $SAMCC_{0.5}$–PMS system to demonstrated that electron transfer in the reaction system only existed on the surface of the catalyst. In *SI Appendix*, Fig. S23, both 2 mM and 20 mM $AgNO_3$ could not inhibit the degradation reaction. This indicated that electron transfer hardly occurred in the reaction solution.

Different model organic pollutants differ in the ability of electron donation. To further prove the previous hypothesis, we further determined the range of organic pollutants that Mo sites can offer a cocatalytic effect in the degradation, with the 5-min degradation effect of various pollutants. The adsorption of various model pollutants by $SAMCC_{0.5}$ and Co–N–C was first excluded in *SI Appendix*, Fig. S24. The adsorption capacity of various model pollutants was less than 20%, and the degradation rate part of subsequent experiments had excluded the adsorption part. Depending on the IP of different model pollutants in Fig. 4 (40–43), $SAMCC_{0.5}$ had little difference in the degradation effect of pollutants with low IP compared with Co–N–C. Starting from phenol (IP = 8.49 eV), the cocatalytic effect of Mo sites on pollutants was significantly improved. Previous studies have indicated that high-valent cobalt systems exhibit improved degradation efficiency for pollutants with low IP due to their relatively weak oxidation potential (44, 45). As a result, for low IP pollutants, Co–N–C systems could effectively degrade these contaminants on their own, and the electron-donating effect of the Mo sites in this system was not pronounced. On the other hand, for pollutants with higher IP, high-valent cobalt systems were less effective in degradation. In this case, the interaction between the pollutant and the Mo site acted as an electron donor, leading to faster regeneration of ROSs in the system and increased resistance to the pollutant. Therefore, the cocatalytic influence of Mo sites in $SAMCC_{0.5}$ was particularly pronounced during the oxidation of pollutants with high IP. In other words, the presence of Mo in $SAMCC_{0.5}$ might broaden the scope of model pollutants that could be oxidized by the single-atom Co catalyst–PMS system, and this scope of pollutants was likely related to their IP. However, there were specific conditions that must be met for this cocatalytic process to occur, such as the adsorption of pollutant molecules on Mo sites. The electron donation effect of Mo sites on pollutants could be effectively applied to substances with an IP ranging from 8.5 to 9.8 eV or even higher. The adsorption of pollutant molecules on Mo sites is an important factor in facilitating the transfer of electrons. However, the strength of the cocatalytic effect of Mo sites is not solely determined by the IP value. Other factors, such as the spatial arrangement of the pollutant molecules and the electronegativity at the adsorption site, also play a significant role in this electron donation process.

Biotoxicity Test of $SAMCC_{0.5}$. In evaluating the suitability of $SAMCC_{0.5}$ as a catalyst in water treatment, its biological toxicity is of paramount importance. To assess this, the effect of $SAMCC_{0.5}$ on human myeloid leukemia mononuclear cells (THP-1), human breast cancer cells (MCF-7 and MDA-MB-231), and Hela cells was evaluated by in vitro cytotoxicity test experiments. The duration of these experiments was set at 48 h, and the concentration of viable cells was determined using the 3-(4,5-dimethylthiazol-2-yl)-2,5-diphenyltetrazolium bromide (MTT) assay at a concentration of 0.5 mg/mL. The results were presented in Fig. 5 *A* and *B* and *SI Appendix*, Figs. S25 and S26. The biotoxicity of $CoCl_2$ was found to be substantial in a dose-dependent manner. At 4.44 mg/L $CoCl_2$, cell viability was found to be generally less than 5%. Notably, the addition of $SAMCC_{0.5}$ resulted in a surprising outcome, with high survival rates observed in all cell lines. The survival rate of THP-1 cells remained close to 60% even when

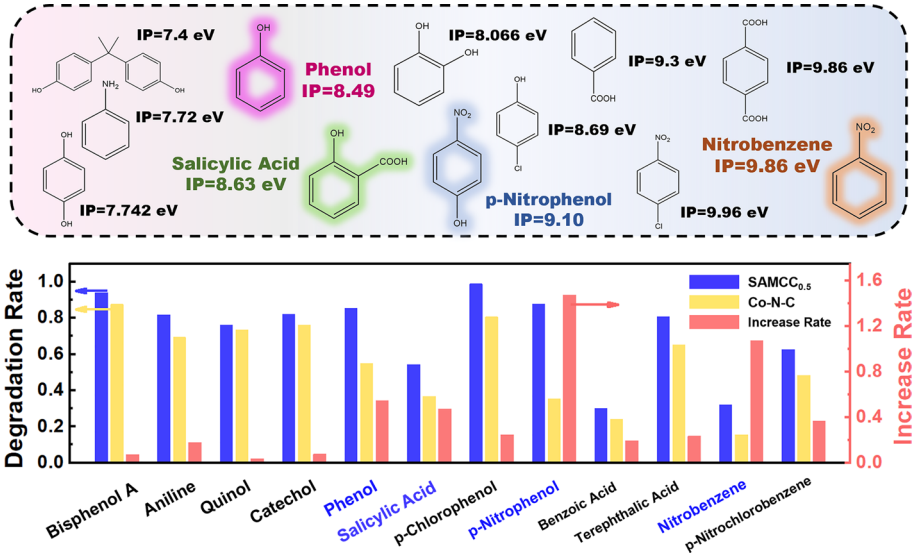

Fig. 4. Degradation rate and increase rate of different model pollutants in the comparison between the $SAMCC_{0.5}$–PMS system and the Co–N–C–PMS system. Dosage: catalyst: 300 mg L^{-1}PMS: 200 mg L^{-1}, aqueous solution: 100 mL, reaction time: 5 min.

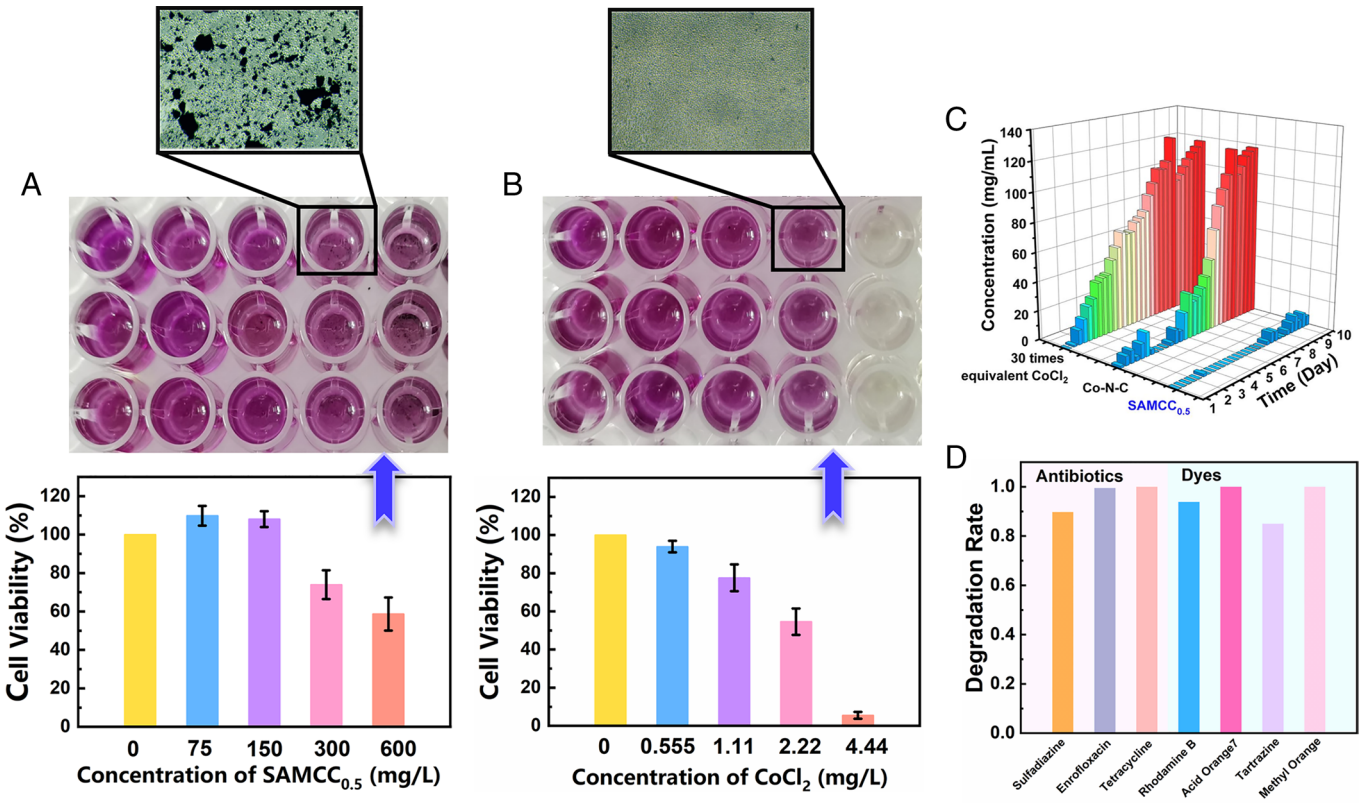

Fig. 5. (*A*) Cell viability of THP-1 under different concentrations of $SAMCC_{0.5}$. Cell culture time: 48 h. The concentration of viable cells with 0.5 mg/mL 3-(4,5-dimethylthiazol-2-yl)-2,5-diphenyltetrazolium bromide (MTT) as inspection agent and cells in the culture medium were observed under a microscope. (*B*) Cell viability of THP-1 under different concentrations of $CoCl_2$. Cell culture time: 48 h. (*C*) Long-term degradation tests of totally 600 mg L^{-1} phenol with 300 mg L^{-1} $SAMCC_{0.5}$, 300 mg L^{-1} Co–N–C, and 30 times equivalent $CoCl_2$ as catalyst. Dosage: PMS: 200 mg L^{-1} every round, phenol: 20 mg L^{-1} every round, aqueous solution: 100 mL. (*D*) Degradation rate of different model pollutants in the $SAMCC_{0.5}$–PMS system. Dosage: catalyst: 300 mg L^{-1}PMS: 200 mg L^{-1}, aqueous solution: 100 mL, reaction time: 30 min, model pollutants: 20 mg L^{-1}.

the cobalt concentration in $SAMCC_{0.5}$ was elevated to match that of 4.44 mg/L $CoCl_2$, at a dose of 600 mg/L (Fig. 5*A*). The results of our experiments demonstrated that $SAMCC_{0.5}$ exhibited low biotoxicity toward MDA-MB-231, Hela, and McF-7 cells, in comparison to the commonly used $CoCl_2$ (*SI Appendix*, Figs. S25 and S26). This made $SAMCC_{0.5}$ an environmentally friendly option for water treatment. Furthermore, $SAMCC_{0.5}$ exhibited higher PMS activation activity than previously reported cobalt catalysts, further highlighting its potential for sustainable use in environmental and biological contexts. The combination of low toxicity and high activity presented a compelling case for the utilization of $SAMCC_{0.5}$ in these fields.

Universality and Stability Testing. The stability of the $SAMCC_{0.5}$ and Co–N–C catalysts was rigorously evaluated through a series of experiments, including cycle tests, long-term degradation experiments, and relevant assessments. To assess the residual metal ions present in the reaction solution, ICP-AES analysis was employed. The results, as reported in *SI Appendix*, Table S3, showed that the residual Co and Mo ions in the solution after the reaction were only 0.39 mg/L and 0.20 mg/L, respectively, for $SAMCC_{0.5}$. This was much lower than the equivalent $CoCl_2$ experiment group, which had residual Co ions of 20.10 mg/L. Compared to $SAMCC_{0.5}$, Co–N–C and Mo–N–C exhibited higher loss of metal ions (0.63 mg/L Co ions for Co–N–C and 2.5 mg/L Mo ions for Mo–N–C) after the reaction. In the cycle tests, $SAMCC_{0.5}$ and Co–N–C were filtered out of the reaction solution after each cycle and washed thoroughly with deionized water. According to *SI Appendix*, Fig. S27, the $SAMCC_{0.5}$ catalyst demonstrated consistent reaction rates during the first two cycles of the five-cycle experiment. Although there was a slight decrease in reaction activity in the latter three cycles, attributed to the impact of the washing process on the catalyst's performance, the $SAMCC_{0.5}$ still exhibited good catalytic activity. Conversely, the cycle experiment for the Co–N–C catalyst in *SI Appendix*, Fig. S28, indicated a declining reactivity with each successive cycle, reflecting its inherently short-lived activity.

In comparison, the long-term experiment provided a clearer illustration of the catalyst's stability in the degradation of organic pollutants within the reaction solution, offering a more comprehensive evaluation of its performance. As shown in Fig. 5*C*, the results of the 10-d long-term degradation experiments with 600 mg/L phenol revealed that the $SAMCC_{0.5}$–PMS system demonstrated superior performance compared to the $CoCl_2$–PMS and Co–N–C–PMS systems. The latter two systems exhibited a significant decline in reactivity after 3 and 13 rounds of testing, respectively, whereas the $SAMCC_{0.5}$–PMS system retained high reactivity over 30 rounds of experiments. The slow reduction of Co^{3+} produced after activation was found to hinder the effective and rapid activation of PMS in the latter stages of the reaction, particularly in the $CoCl_2$–PMS system. In the case of the Co–N–C–PMS system, a similar decline in reactivity was observed. The unique advantage of the $SAMCC_{0.5}$–PMS system lied in the Mo element, which played a crucial role in the Co^{2+}/Co^{3+} cycle. In the $SAMCC_{0.5}$–PMS system, the reduction of Co sites was facilitated by the transfer of electrons from organic pollutants via the Mo sites and conjugated skeleton. The $SAMCC_{0.5}$, with its unique feature, maintained high activity throughout the extended

degradation process, which provided a significant advantage compared to catalysts lacking a cocatalytic system. Moreover, the $SAMCC_{0.5}$–PMS system exhibited broad universality in its ability to degrade a wide range of pollutants. This was evidenced by the results of the degradation experiments with complex model pollutants, as shown in Fig. 5*D*. Within 30 min, the degradation rate of various antibiotics and dyes, including sulfadiazine, enrofloxacin, tetracycline, Rhodamine B, acid orange 7, tartrazine, and methyl orange, reached 90%. This demonstrated the system's ability to effectively oxidize organic compounds with complex structures. In order to further verify the performance of the $SAMCC_{0.5}$–PMS system in pollutants degradation, actual industrial wastewater was used as a reaction raw material and reaction solution in *SI Appendix*, Table S4, with chemical oxygen demand (COD) as the index. For the sample from biochemical wastewater, the COD decreased by 127 mg/L. And for the actual wastewater from Beijing Construction Engineering Group Co., Ltd., the COD decreased by 95 mg/L after treatment.

Conclusions

In this article, we synthesized bimetallic site SACs that were well suited to environmental remediation and explored the interactions between metal sites and pollutants. The individual distribution of metal sites in $SAMCC_{0.5}$ ensured both excellent stability and high reactivity. The addition of Mo sites significantly increased the catalytic performance of Co–N–C in the initial 10 min of the reaction, resulting in a 19.4-fold increase in the degradation rate of phenol compared to the $CoCl_2$–PMS group. Furthermore, the degradation efficacy of $SAMCC_{0.5}$ was not impacted by variations in pH or the presence of ions, even at extreme pH = 1 or 13. In the 10-d long-term experiments, $SAMCC_{0.5}$ exhibited stable, long-term activation, as a result of the cocatalytic effect of Mo sites, leading to the complete degradation of 600 mg/L of phenol. And the cocatalytic effect of Mo sites was proved to be the guidance of the electron transportation from pollutants to Co sites. The electron transfer facilitated by Mo sites was particularly well suited for pollutants with IP ranging from 8.5 to 9.8 eV or higher. This cocatalytic effect of Mo sites represented a significant advancement in the study of cocatalysts, offering a unique perspective compared to previous work on the cocatalytic effect of the Mo element. Furthermore, this research provides valuable insights into the interaction between different metal sites in SACs, leading to increased metal utilization and reduced biotoxicity of the catalyst. With its environmentally friendly and low biotoxicity properties, $SAMCC_{0.5}$ holds great potential for a range of applications in fields such as environmental remediation, biology, medicine, and catalysis.

Materials and Methods

Preparation of Catalysts. First, 1,10-phenanthroline and $Co(CH_3COO)_2$ were dissolved in 20 mL ethanol, and $(NH_4)_2MoO_4$ was dissolved in 5 mL deionized water. After mixing the above solution, the solution was treated with ultrasound for 30 min. In the second step, $Mg(OH)_2$ was added to the mixed solution and treated with ultrasound for 30 min. Subsequently, the mixture was placed in a vacuum oven to dry after rotary evaporation. The dried sample was then ground and calcined in a tube furnace at 700 °C for 120 min. The product was stirred in 1M of HNO_3 for 4 h to leach $Mg(OH)_2$, MgO, and any possible metal or oxide. After washing with ultrapure water five times, the solid was dried at 60 °C overnight. Here, we name the resulting catalyst SAMCC, and the amount of relevant raw materials in catalyst synthesis was indicated in *SI Appendix*, Figs. S1 and S2. In the synthesis of Co–N–C, $(NH_4)_2MoO_4$ was not used while other processing methods were consistent. In the synthesis of Mo–N–C, $Co(CH_3COO)_2$ was not used while other processing methods were consistent. In the synthesis of N–C, $Co(CH_3COO)_2$ was replaced by the same amount of acetic acid, and other metal salts were not added.

Catalytic Effect Test in Fenton-Like Reaction. Typically, 30 mg catalyst was added into 100 mL phenol solution (20% wt. %). Then, NaOH and H_2SO_4 were added to adjust pH if needed, and various inorganic salts were also added at this time if needed. Twenty mg of PMS was added at the beginning of the experiment. After sampling at different time points, it was filtered with a filter head, and then, methanol was added to quench the reaction. The concentration of phenol was detected by HPLC.

Cell Culture and Cell Viability Assay. The Hela and MDA-MB-231 cell lines were obtained from China Center for Type Culture Collection (CCTCC). These cell lines were cultured in Dulbecco's modified Eagle's medium (DMEM; KeyGEN Biotech) with 10% fetal bovine serum (FBS; ExCell Bio). The cells were maintained at 37 °C in a humidified incubator with 95% air and 5% CO_2.

Cells (5×10^5 cells/well) were seeded in 96-well plates overnight and then treated with various concentrations of tested samples. The concentrations were 0, 75, 150, 300, and 600 mg, respectively, for $SAMCC_{0.5}$. The concentrations were 0, 0.555, 1.11, 2.22, and 4.44 mg, respectively, for $CoCl_2$. After 48 h, the original medium was removed, and 100 μL fresh medium containing 0.5 mg/mL 3-(4,5-dimethylthiazol-2-yl)-2,5-diphenyltetrazolium bromide (MTT) was added to each well for 4 h at 37 °C. Then, the medium was replaced with 150 μL of DMSO to dissolve the formazan. Absorbance was measured at 570 and 630 nm using a microplate reader (Molecular Devices). All the experiments were performed in three independent replicates.

Statistical Analysis. All data were gained directly from the source experiment and processed using Origin. All experiments were carried out in duplicate. Full details for DFT computations, control experiments, and materials characterizations were introduced in *SI Appendix*.

Data, Materials, and Software Availability. All study data are included in the article and/or *SI Appendix*.

ACKNOWLEDGMENTS. This work was supported by the National Natural Science Foundation of China (Nos. 22176060 and 41876189) and sponsored by the Program of Shanghai Academic/Technology Research Leader (23XD1421000). Project supported by Shanghai Municipal Science and Technology Major Project (Grant No. 2018SHZDZX03) and the Program of Introducing Talents of Discipline to Universities (B16017). Science and Technology Commission of Shanghai Municipality (20DZ2250400). The Fundamental Research Funds for the Central Universities (222201717003). We thank Research Center of Analysis and Test of East China University of Science and Technology for the help on the characterization.

1. M.-H. Zhang, H. Dong, L. Zhao, D.-X. Wang, D. Meng, A review on Fenton process for organic wastewater treatment based on optimization perspective. *Sci. Total Environ.* **670**, 110–121 (2019).
2. J. P. Sumpter, A. C. Johnson, Lessons from endocrine disruption and their application to other issues concerning trace organics in the aquatic environment. *Environ. Sci. Technol.* **39**, 4321–4332 (2005).
3. W.-W. Li, H.-Q. Yu, Z. He, Towards sustainable wastewater treatment by using microbial fuel cells-centered technologies. *Energy Environ. Sci.* **7**, 911–924 (2014).
4. W. Liu *et al.*, Efficient hydrogen production from wastewater remediation by piezoelectricity coupling advanced oxidation processes. *Proc. Natl. Acad. Sci. U.S.A.* **120**, e2218813120 (2023).
5. S. Liang *et al.*, Fe^{2+}/HClO reaction produces $FeIVO^{2+}$: An enhanced advanced oxidation process. *Environ. Sci. Technol.* **54**, 6406–6414 (2020).
6. A. Goswami, J.-Q. Jiang, M. Petri, Treatability of five micro-pollutants using modified Fenton reaction catalysed by zero-valent iron powder (Fe (0)). *J. Environ. Chem. Eng.* **9**, 105393 (2021).
7. S. Lu, L. Liu, H. Demissie, G. An, D. Wang, Design and application of metal-organic frameworks and derivatives as heterogeneous Fenton-like catalysts for organic wastewater treatment: A review. *Environ. Int.* **146**, 106273 (2021).
8. M. Du *et al.*, Sustainable activation of peroxymonosulfate by the Mo (IV) in MoS_2 for the remediation of aromatic organic pollutants. *Chin. Chem. Lett.* **31**, 2803–2808 (2020).
9. C. Dong *et al.*, Research progress of photocatalysis based on highly dispersed titanium in mesoporous SiO_2. *Chin. Chem. Lett.* **30**, 853–862 (2019).
10. Y. Zhen *et al.*, Facile preparation of α-MnO_2 nanowires for assembling free-standing membrane with efficient Fenton-like catalytic activity. *Chin. Chem. Lett.* **34**, 107664 (2023).
11. A. Wang, J. Li, T. Zhang, Heterogeneous single-atom catalysis. *Nat. Rev. Chem.* **2**, 65–81 (2018).
12. H. Zhang, G. Liu, L. Shi, J. Ye, Single-atom catalysts: Emerging multifunctional materials in heterogeneous catalysis. *Adv. Energy Mater.* **8**, 1701343 (2018).

13. S. Ding, M. J. Hülsey, J. Perez-Ramirez, N. Yan, Transforming energy with single-atom catalysts. *Joule* **3**, 2897–2929 (2019).
14. A. Beniya, S. Higashi, Towards dense single-atom catalysts for future automotive applications. *Nat. Catal.* **2**, 590–602 (2019).
15. X. Li *et al.*, Single cobalt atoms anchored on porous N-doped graphene with dual reaction sites for efficient Fenton-like catalysis. *J. Am. Chem. Soc.* **140**, 12469–12475 (2018).
16. B. Wang *et al.*, A site distance effect induced by reactant molecule matchup in single-atom catalysts for fenton-like reactions. *Angew. Chem. Int. Ed.* **134**, e202207268 (2022).
17. J. Xu *et al.*, Organic wastewater treatment by a single-atom catalyst and electrolytically produced H_2O_2. *Nat. Sustain.* **4**, 233–241 (2021).
18. Y. Xiong *et al.*, Single-atom Fe catalysts for Fenton-Like reactions: Roles of different N species. *Adv. Mater.* **34**, 2110653 (2022).
19. F. Chen *et al.*, Molecular engineering toward pyrrolic N-rich M-N4 (M= Cr, Mn, Fe Co, Cu) single-atom sites for enhanced heterogeneous fenton-like reaction. *Adv. Funct. Mater.* **31**, 2007877 (2021).
20. Y. Yin *et al.*, Boosting Fenton-like reactions via single atom Fe catalysis. *Environ. Sci. Technol.* **53**, 11391–11400 (2019).
21. M. Chen *et al.*, Efficient degradation of organic pollutants by low-level Co^{2+} catalyzed homogeneous activation of peroxymonosulfate. *J. Hazard. Mater.* **371**, 456–462 (2019).
22. P. Hu, M. Long, Cobalt-catalyzed sulfate radical-based advanced oxidation: A review on heterogeneous catalysts and applications. *Appl. Catal. B.* **181**, 103–117 (2016).
23. F. Rivas, O. Gimeno, T. Borallho, Aqueous pharmaceutical compounds removal by potassium monopersulfate. Uncatalyzed and catalyzed semicontinuous experiments. *Chem. Eng. J.* **192**, 326–333 (2012).
24. X. Lu *et al.*, Bioinspired copper single-atom catalysts for tumor parallel catalytic therapy. *Adv. Mater.* **32**, 2002246 (2020).
25. X. Liu, Y. Pei, M. Cao, H. Yang, Y. Li, Highly dispersed copper single-atom catalysts activated peroxymonosulfate for oxytetracycline removal from water: Mechanism and degradation pathway. *Chem. Eng. J.* **450**, 138194 (2022).
26. Y. Qi *et al.*, Novel lignin-based single atom catalysts as peroxymonosulfate activator for pollutants degradation: Role of single cobalt and electron transfer pathway. *Appl. Catal. B.* **286**, 119910 (2021).
27. K. Zhao *et al.*, Enhanced chlorinated pollutant degradation by the synergistic effect between dechlorination and hydroxyl radical oxidation on a bimetallic single-atom catalyst. *Environ. Sci. Technol.* **55**, 14194–14203 (2021).
28. Y. Yang, G. Banerjee, G. W. Brudvig, J.-H. Kim, J. J. Pignatello, Oxidation of organic compounds in water by unactivated peroxymonosulfate. *Environ. Sci. Technol.* **52**, 5911–5919 (2018).
29. D. L. Ball, J. O. Edwards, The kinetics and mechanism of the decomposition of Caro's acid I. *J. Am. Chem. Soc.* **78**, 1125–1129 (1956).
30. E. Lipczynska-Kochany, G. Sprah, S. Harms, Influence of some groundwater and surface waters constituents on the degradation of 4-chlorophenol by the Fenton reaction. *Chemosphere* **30**, 9–20 (1995).
31. M. Sánchez-Polo, R. Ocampo-Pérez, J. Rivera-Utrilla, A. J. Mota, Comparative study of the photodegradation of bisphenol A by HO, SO_4^- and CO_3^-/HCO_3 radicals in aqueous phase. *Sci. Total Environ.* **463**, 423–431 (2013).
32. X. Liang *et al.*, Coordination number dependent catalytic activity of single-atom cobalt catalysts for fenton-like reaction. *Adv. Funct. Mater.* **32**, 2203001 (2022).
33. J. Al-Nu'airat *et al.*, Reaction of phenol with singlet oxygen. *Phys. Chem. Chem. Phys.* **21**, 171–183 (2019).
34. Y. Zhou *et al.*, Activation of peroxymonosulfate by phenols: Important role of quinone intermediates and involvement of singlet oxygen. *Water Res.* **125**, 209–218 (2017).
35. T. Yang, S. Fan, Y. Li, Q. Zhou, Fe-N/C single-atom catalysts with high density of Fe-N_x sites toward peroxymonosulfate activation for high-efficient oxidation of bisphenol A: Electron-transfer mechanism. *Chem. Eng. J.* **419**, 129590 (2021).
36. H. Lee *et al.*, Activation of persulfates by carbon nanotubes: Oxidation of organic compounds by nonradical mechanism. *Chem. Eng. J.* **266**, 28–33 (2015).
37. B.-C. Huang, G.-X. Huang, J. Jiang, W.-J. Liu, H.-Q. Yu, Carbon-based catalyst synthesized and immobilized under calcium salt assistance to boost singlet oxygen evolution for pollutant degradation. *ACS Appl. Mater. Interfaces.* **11**, 43180–43187 (2019).
38. Y. Zong *et al.*, Unraveling the overlooked involvement of high-valent cobalt-oxo species generated from the cobalt (II)-activated peroxymonosulfate process. *Environ. Sci. Technol.* **54**, 16231–16239 (2020).
39. X. Liu *et al.*, Graphene oxide-supported three-dimensional cobalt–nickel bimetallic sponge-mediated peroxymonosulfate activation for phenol degradation. *ACS ES&T Eng.* **1**, 1705–1714 (2021).
40. Q. Wang *et al.*, Two-dimensional ultrathin perforated Co_3O_4 nanosheets enhanced PMS-Activated selective oxidation of organic micropollutants in environmental remediation. *Chem. Eng. J.* **427**, 131953 (2022).
41. A. R. L. da Silva, A. J. Dos Santos, C. A. Martínez-Huitle, Electrochemical measurements and theoretical studies for understanding the behavior of catechol, resorcinol and hydroquinone on the boron doped diamond surface. *RSC Adv.* **8**, 3483–3492 (2018).
42. R. Joshi, T. K. Ghanty, T. Mukherjee, Substituent effect on ionization potential, O-H bond dissociation energy and intra-molecular hydrogen bonding in salicylic acid derivatives. *J. Mol. Struct.* **948**, 47–54 (2010).
43. D. R. Lide, *CRC Handbook of Chemistry and Physics* (CRC Press, **vol. 85**, 2004).
44. B. Liu *et al.*, Peroxymonosulfate activation by cobalt (II) for degradation of organic contaminants via high-valent cobalt-oxo and radical species. *J. Hazard. Mater.* **416**, 125679 (2021).
45. B. Liu *et al.*, Insights into the oxidation of organic contaminants by Co (II) activated peracetic acid: The overlooked role of high-valent cobalt-oxo species. *Water Res.* **201**, 117313 (2021).